



Electrical Source Imaging of Somatosensory Evoked Potentials from Intracranial EEG Signals

Adam Kalina¹ · Petr Jezdik² · Petr Fabera¹ · Petr Marusic¹ · Jiri Hammer¹

Received: 6 September 2022 / Accepted: 24 July 2023 / Published online: 29 August 2023
© The Author(s), under exclusive licence to Springer Science+Business Media, LLC, part of Springer Nature 2023

Abstract

Stereoelectroencephalography (SEEG) records electrical brain activity with intracerebral electrodes. However, it has an inherently limited spatial coverage. Electrical source imaging (ESI) infers the position of the neural generators from the recorded electric potentials, and thus, could overcome this spatial undersampling problem. Here, we aimed to quantify the accuracy of SEEG ESI under clinical conditions. We measured the somatosensory evoked potential (SEP) in SEEG and in high-density EEG (HD-EEG) in 20 epilepsy surgery patients. To localize the source of the SEP, we employed standardized low resolution brain electromagnetic tomography (sLORETA) and equivalent current dipole (ECD) algorithms. Both sLORETA and ECD converged to similar solutions. Reflecting the large differences in the SEEG implantations, the localization error also varied in a wide range from 0.4 to 10 cm. The SEEG ESI localization error was linearly correlated with the distance from the putative neural source to the most activated contact. We show that it is possible to obtain reliable source reconstructions from SEEG under realistic clinical conditions, provided that the high signal fidelity recording contacts are sufficiently close to the source of the brain activity.

Significance

SEEG-based ESI is able to improve the localization of epileptogenic and functional networks, beyond the vicinity of the intracerebral recording electrodes.

Handling Editor: Christian-G. Bénar.

Petr Marusic and Jiri Hammer are joint senior authors.

✉ Adam Kalina
adam.kalina@fnmotol.cz

✉ Jiri Hammer
jiri.hammer@lfmotol.cuni.cz

Petr Jezdik
petr.jezdik@fel.cvut.cz

Petr Fabera
petr.fabera@fnmotol.cz

Petr Marusic
petr.marusic@fnmotol.cz

¹ Department of Neurology, Second Faculty of Medicine, Charles University and Motol University Hospital (Full Member of the ERN EpiCARE), V Uvalu 84, 150 06 Prague 5, Czechia

² Department of Measurement, Faculty of Electrical Engineering, Czech Technical University in Prague, Technicka 2, 166 27 Prague 6, Czechia

Keywords Electrical source localization (ESL) · Inverse problem · Somatosensory evoked potential (SEP, SSEP) · Intracranial EEG (iEEG) · High-density EEG (HD-EEG) · Stereo-EEG (SEEG)

Introduction

Stereoelectroencephalography (SEEG) is a brain signal recording technique that uses a system of intracerebral electrodes. Similar to electrocorticography (ECoG), SEEG measures intracranial electric potential changes, but unlike ECoG grids or stripes, SEEG electrodes penetrate the brain parenchyma and are thus, able to target almost every cerebral structure, including gyral crowns, bottom of sulci, white matter, mesial brain structures and insula. It is predominantly used in patients with pharmaco-resistant epilepsy for precise localization and delineation of the epileptogenic network and functional surrounding areas (George et al. 2020; Minotti et al. 2018). Furthermore, intracranial EEG (iEEG), composed of both ECoG and SEEG, from epilepsy patients has also been successfully applied in cognitive neuroscience research (Parvizi and Kastner 2018).

Despite its high temporal and spectral resolution, spatial precision, signal-to-noise ratio and robustness against artifacts; spatial undersampling remains the main limitation of SEEG (Isnard et al. 2018). Currently, the prevailing clinical, as well as, neuroscientific approach in the analysis of SEEG electrical brain activity focuses on visual inspection of the activations directly at the electrode contacts. Brain regions implanted during SEEG exploration are chosen carefully based on the electro-clinical hypothesis about the seizure onset zone in individual patients. However, in cases where the lesion is more focal than anticipated or in cases of incorrect hypothesis, the electrodes may not be positioned optimally and in an extreme case may be even misplaced with respect to the source. Consequently, a method that could define sources beyond the close vicinity of the SEEG recording electrodes would be highly desirable and could lead to further improvements in localization of epileptogenic (Ramantani et al. 2013), and functional (Bastin et al. 2017; Völker et al. 2018) networks.

Electrical source imaging (ESI) solves the inverse problem of finding hidden neural sources of brain activity from signals recorded by the electrodes (or sensors, in general), see (Michel et al. 2004; Michel and Brunet 2019) for a comprehensive review). ESI is most typically used with scalp EEG or MEG (magnetoencephalography). Reports of ESI using SEEG (but also ECoG) are infrequent, presumably because the SEEG signal is generally considered to be the local field potential. In fact, the iEEG is itself often used as the ground truth source location for scalp EEG-based ESI (Bai et al. 2007; Koessler et al. 2010; Tamilya et al. 2019). This notion of spatial focality is further enhanced by the prevalent use of bipolar montage in clinical practice,

subtracting the activity from neighboring contacts of the same electrode and thus, canceling the far-field sources that would otherwise contribute to both contacts by approximately the same amount, e.g. (Vlček et al. 2020). However, if the iEEG is referenced to a common average, then the far field sources are preserved, thus enabling their reconstruction.

The majority of iEEG-based ESI studies have focused on numerically simulated signals using either ECoG electrodes (Zhang et al. 2008; Dümpelmann et al. 2009, 2012; Cho et al. 2011; Lie et al. 2015; Pascarella et al. 2016; Cosandier-Rimele et al. 2017; Todaro et al. 2019) or SEEG electrodes (Chang et al. 2005; Caune et al. 2014; Hosseini et al. 2018; Le Cam et al. 2014, 2017, 2019). The simulated signal has the profound advantage of a clearly defined source location, a temporal profile and the possibility to manipulate the signal-to-noise ratio (SNR). Although such studies are key first steps for method validation and gaining further insights, an open question is how much the simulated signals resemble the activity measured with physiological iEEG signals in the real brain. In particular, the brain activity in the simulation studies is typically modeled as a single dipolar source with additive noise; the noise on different electrode contacts is often modeled as Gaussian, white and uncorrelated—characteristics that do not occur under physiological conditions.

Fewer studies deal with ESI based on physiological (i.e., not numerically simulated) iEEG signals (Yvert et al. 2005; Zhang et al. 2008; Dümpelmann et al. 2012; Ramantani et al. 2013; Caune et al. 2014; Alhilani et al. 2020; Lin et al. 2021) and are often limited to single-case reports. Importantly, methods of ESI using real iEEG signals were successful in localizing the irritative zone, seizure onset zone and even predict the outcome of brain resection (Ramantani et al. 2013, 2014; Alhilani et al. 2020; Satzer et al. 2022). Studies using different evoked potentials, for example, auditory evoked potentials (AEPs), were able to correctly reconstruct their origin and even their time course (Yvert et al. 2005; Sammler et al. 2013; Korzyukov et al. 2007).

Currently, a systematic evaluation of SEEG-based source localization and its determinants under fully realistic experimental conditions and with a higher sample size of patients is lacking. To address the accuracy of ESI under physiological settings, it is necessary to solve the issue of the unknown source location (the so-called “ground truth”). Thus, an experimental design with known (or independently estimated) “ground truth” locations of the sources is required.

In this study, we aimed to analyze which parameters of SEEG recordings most influence the source reconstruction and thereby, confirm (or reject) some of the predictions from

studies using numerical simulations (Dümpelmann et al. 2009, 2012; Caune et al. 2014; Le Cam et al. 2014). Is it the distance from the putative source to the closest SEEG electrode contacts (Le Cam et al. 2014), the number of highly active contacts/electrodes (Caune et al. 2014), or the spatial arrangement around the putative source (Le Cam et al. 2019)? How far can SEEG detect sources (Hosseini et al. 2018)?

To this end, we compared the localization results of somatosensory evoked potential (SEP) obtained from HD-EEG ESI and SEEG ESI for 20 different patients. We extracted different parameters of SEEG recordings to address the above research questions about the determinants of the ESI localization results from SEEG signals.

The location of the putative source of SEP, the “ground truth” source location to which the SEEG ESI was compared, was estimated from a HD-EEG recording (Fig. 1). Notably, the HD-EEG measurements were not concurrent with the SEEG, but took place before the SEEG implantation (due to technical and clinical limitations). We would like to underline that the position of the “ground truth” is only estimated and subject to limitations, resulting from this estimation. Throughout the manuscript, we will systematically use the term “ground truth” source location in quotes to remind of this limitation. We specifically exploited the SEP, because the SEP after median nerve stimulation is a well established source of electrical activity in the human brain originating predominantly in the postcentral gyrus (Hari and Forss 1999) that is also easily detectable with scalp EEG (Grimm et al. 1998). We used this *a-priori* knowledge about SEP location to visually verify the “ground truth” location of the putative source from HD-EEG ESI.

For the inverse solutions from SEEG, we selected two different, widely used methods: (1) sLORETA (standardized

LOW REsolution brain electromagnetic TomogrAphy, (Pascual-Marqui 2002) and (2) equivalent current dipole (ECD) (Hämäläinen et al. 1993). Choice of the inverse solution method is typically dependent on assumptions that can be made about the nature of the signal source. For focal sources, such as the early response of SEP, where only one or a few brain areas are activated (Lee and Seyal 1998; Towle et al. 2003), the ECD technique with one dipole can yield reliable results (Pellegrino et al. 2018; Scherg and Von Cramon 1985). The sLORETA is a distributed source model, unbiased by the number of *a priori* assumed sources and, in principle, can provide a good explanation for recorded data even if multiple sources are in action. Importantly, both inverse solution methods were often used in iEEG-based ESI: ECD (Alhilani et al. 2020; Caune et al. 2014; Tamilia et al. 2019), and sLORETA (Cho et al. 2011; Dümpelmann et al. 2012; Lie et al. 2015).

Here, we demonstrate that SEEG may facilitate reliable source reconstruction beyond that of the closest electrodes and clarify the conditions to achieve optimal ESI results.

Materials and Methods

The aim of this study was to assess the localization accuracy of SEEG-based ESI. The “ground-truth” location of the SEP source, to which the SEEG-ESI results were compared, was taken from the SEP source estimated by sLORETA from HD-EEG recordings and the plausibility of this estimation was carefully visually inspected. For the source reconstructions, we used “off the shelf” localization methods implemented in the Brainstorm software package (Tadel et al. 2011) version May 2021. The

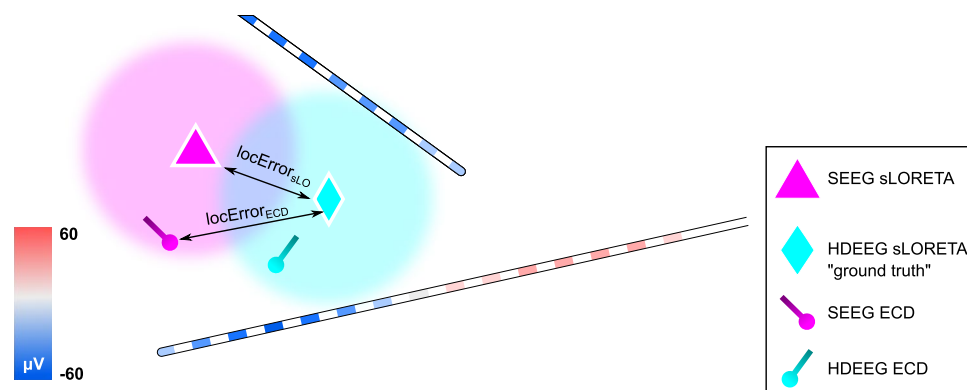


Fig. 1 A scheme of ESI of SEP. We used two different signals for ESI: SEEG and HD-EEG from the same patient. The signals were not, however, measured concurrently. We computed source locations using two different algorithms: ECD and sLORETA. Importantly, the “ground truth” location of the SEP was taken from the HD-EEG sLORETA solution (cyan diamond) and carefully visually inspected

and verified that it originated in the vicinity of the posterior wall of the central sulcus. The regions explored by SEEG were not optimized for detection of SEP, but were solely based on the needs of clinical diagnostics. The localization errors of SEEG-based ESI for both methods were compared to this one, unique “ground truth” solution

results were exported and further analyzed and visualized in MATLAB (The MathWorks, Natick, MA, USA).

Participants

Twenty patients (13 females, mean age 31 years, age range 19–54 years) with pharmaco-resistant epilepsy participated in the study (see Table 1 for details). One patient (P6) had two consecutive SEEG implantations resulting in 21 implantations in total. The patients were recruited at Motol University Hospital, Prague, Czech Republic and all gave informed consent approved by the local ethics committee. All patients underwent high density EEG (HD-EEG) recording with 256 scalp electrodes prior to stereo-EEG (SEEG) implantation. Concurrent recording of HD-EEG and SEEG was not possible due to technical reasons.

SEEG Recordings

The implantation sites were selected solely according to clinical indication. Details of the implantation sites are summarized in Table 1. Six to seventeen semi-rigid electrodes (DIXI Medical Instruments) were implanted per patient in cortical areas depending on the suspected origin of their seizures. Each electrode had a diameter of 0.8 mm and consisted of 8 to 18 contacts of 2 mm length and 1.5 mm inter-contact distance. Electrode contacts were identified from post-implantation CT coregistered with pre-implantation MRI using BioImage Suite 3.0 (Papademetris et al. 2006) and loaded into Brainstorm. Post-implantation MRI was available in 13 patients and we observed no shifts in the brain tissue nor hemorrhages resulting in tissue displacement, which could have impacted the localization results.

The SEEG signal was recorded using two different video-EEG monitoring systems: Natus NicoletOne with 128 recording channels (in 13 patients, P1–P13) or Natus Quantum with 256 recording channels available (in 7

Table 1 List of participants

Alias	Sex (age)	SEEG system $N_{elec}/N_{impl}/N_{rec}/N_{used}$	Site of implantation	Pathology
P1	F (23)	12/137/126/119	Bilateral temporal	FCD 1B
P2	M (19)	12/143/118/112	Right opercular	FCD 2B
P3	F (33)	11/135/124/118	Left frontal	Gliosis
P4	F (28)	10/116/100/94	Right temporal	FCD 1 A
P5	F (29)	11/149/126/124	Right pericentral	FCD 2B
P6-1	F (22)	10/137/109/105	Left operculo-insular	Not operated
P6-2	F (22)	6/88/80/72	Left operculo-insular	Not operated
P7	F (25)	12/139/118/115	Right operculo-insular	Gliosis
P8	M (54)	9/133/119/117	Left frontal	FCD 2B
P9	F (42)	11/140/121/118	Right temporal	FCD 2B
P10	M (33)	12/189/126/126	Bilateral pericentral	FCD 2B
P11	M (23)	14/212/126/118	Right frontal	Gliosis
P12	F (28)	14/173/126/125	Right opercular	Not operated
P13	M (33)	15/200/126/125	Left temporal	FCD 1B
P14	F (46)	12/160/151/148	Right temporo-insular	FCD 1C
P15	F (22)	16/146/131/130	Left parietal + bifrontal	Not operated
P16	M (22)	11/141/126/125	Left opercular	FCD 2B
P17	F (24)	17/227/199/198	Right temporo-insular	Complex malformation
P18	F (44)	18/224/214/206	Right opercular	Not operated
P19	F (38)	10/131/118/118	Right operculo-insular	Not operated
P20	M (37)	9/117/109/108	Left pericentral	Gliosis

N_{elec} number of implanted electrodes, N_{impl} total number of intracranial contacts, N_{rec} number of recorded channels (significantly lower in P1–P13 where only 128 channels could be recorded), N_{used} number of channels used for analysis after artifact and IED channel rejection. P6 was implanted twice, designated by using P6-1 and P6-2 for the first and second implantation, respectively. Site of implantation refers primarily to the main target of SEEG exploration, not the whole extent. Opercular region refers to the parts of the parietal, frontal and temporal lobes covering the insula. Pericentral region refers to the precentral and postcentral gyrus.

patients, P14–P20). In patients P1–P13 only the 128 channel recording was available. Therefore, some electrodes were not recorded, mostly those located in the white matter. The data were sampled at 512 Hz with usable frequency bands 0.16–134 Hz for NicoletteOne or 2048 Hz with usable frequency bands 0.01–682 Hz for Quantum. For each patient, the reference electrode contact was located in the white matter. Note that the Brainstorm computes common average reference prior to the ESI computation.

HD-EEG Recordings

HD-EEG signal was recorded using ANT Neuro monitoring system with 256 electrode caps (Duke system), the individual positions of the contacts on the cap were obtained using an optical tracking system (Xensor, ANT Neuro) and loaded into Brainstorm to match with the patient-specific MRI. The data were sampled at 2048 Hz with usable frequency bands 0–409.6 Hz and a hardware defined common average reference. Impedance of HD-EEG electrodes was kept below 10 kOhm during the whole recording.

Stimulation of SEP (Same for Both HD-EEG and SEEG)

The median nerve was stimulated at the wrist using the Synergy Nicolet EMG system with at least 512 impulses on each side (range 512–1024, median 512), with a 2 Hz frequency, 0.2 ms pulse width and an amplitude adjusted individually to elicit a motor response (range 2.7–7.9 mA, median 4.5 mA). Patients were lying supine with eyes closed and were instructed to stay still and relaxed. At the beginning of each SEP stimulation, a trigger mark was transmitted from the SEP electrical stimulator to the respective SEEG or HD-EEG amplifier for subsequent data alignment.

Signal Preprocessing (Same for Both HD-EEG and SEEG)

Signals from both SEEG and HD-EEG recordings were aligned on the trigger marks (beginning of the median nerve stimulation), epoched in a 2 s long window centered on the trigger mark and averaged. The longer epoch of 2 s was used to avoid filtration artifacts at the edges of the window. A smaller window of [– 200; 400 ms] was then used as the input to the ESI algorithms. No epoch rejection was performed. Artifacts or broken channels were excluded in both SEEG and HD-EEG datasets based on visual inspection. Channels with abundant interictal epileptiform discharges, identified by experienced neurologists, were excluded from the analysis of the SEEG as well. The raw, epoched EEG data (for both HD-EEG and SEEG) were filtered at a frequency between 10 and 30 Hz (we used a zero-phase shift

FIR filter with Kaiser window implemented in Brainstorm software). The choice of frequency band was similar to that documented (Houzé et al. 2011; Lascano et al. 2014), where a high-pass filter of 10 Hz for source localization of SEP in HD-EEG was used. Here we set the upper cut-off at 30 Hz to filter out the 50 Hz artifact, as the recordings took place in an unshielded room (i.e., without a Faraday cage). Both the HD-EEG and SEEG recordings were converted to a common average reference before the projection to the source domain.

Electrical Source Imaging (Same for Both HD-EEG and SEEG)

We used two different ESI models for computing the inverse solutions: sLORETA and ECD. The sLORETA (Pascual-Marqui 2002) is a spatially distributed model based on the minimum-norm least-square solution and constraining the source as well as noise variances. Here, we used default Brainstorm settings (Tadel et al. 2011), in particular a regularization parameter equal to three, depth weighting equal to 0.5, regularize noise covariance equal to 0.1 and unconstrained orientation of dipolar sources at each grid point. Unconstrained orientation of dipoles were used since we were also interested in the potentially confounding effects of activity of other brain structures. The ECD (Hämäläinen et al. 1993) is a source localization method based on dipole scanning, which iteratively searches the brain space and fits a single dipole with an unconstrained orientation. Here again, we used the default implementation in Brainstorm (i.e., median eigenvalue for noise covariance regularization). The assumption of a single dipole is well justified for the early response SEP (Lee and Seyal 1998; Towle et al. 2003). Both algorithms were successfully used in a number of studies localizing brain activity, also from iEEG (Lie et al. 2015; Alhilani et al. 2020). The source localization analyses were carried out in the Brainstorm software package (version May 2021) (Tadel et al. 2011).

Forward Modeling: SEEG and HD-EEG

The boundary element method (BEM) was used to construct the lead fields based on realistic head models derived from individual patient's pre-implantation MRI images. Specifically, the software package CAT12 (Dahnke et al. 2013) was used for segmentation into the head mask, outerskull, inner skull and brain. The resulting surfaces were then used by OpenMEEG (Gramfort et al. 2010) to create the BEM head models with the source based on MRI volume with an isotropic grid of 4 mm resolution sampling the full brain volume, to also account for deep brain regions (Alhilani et al. 2020). Brainstorm's default conductivities for scalp, skull and brain were used with their relative ratio of 1:0.0125:1,

respectively with 1922 vertices in each layer (scalp, inner skull, outer skull) and 15 000 vertices in the cortex.

Time of Source Localization: SEEG and HD-EEG

The source localization was applied at a single time point typically corresponding to the peak of the global field power (GFP) of the SEP in SEEG or HD-EEG (Lascano et al. 2014). In more detail, the peak of the GFP corresponding to an early stable response was used (Houzé et al. 2011). In few cases where there was no clear peak of GFP for the SEEG, we used the time-point from HD-EEG.

Comparison of SEP Sources from SEEG and HD-EEG

We used two measures to assess the results of ESI localization from the SEEG: (1) the localization error for both sLORETA and ECD and (2) the spatial overlap for the distributed sLORETA solutions.

We estimated the putative, “ground truth” source location of SEP from HD-EEG recordings individually for each patient using the sLORETA algorithm. The results of the HD-EEG inverse solutions were carefully visually inspected to confirm their localization in the central sulcus by an expert on cortical anatomy. In more detail, ESI results from HD-EEG were visually validated based on Atlas of the Human Brain 5th edition (Mai et al. 2016). All results were concordant with presumed localization in the posterior wall of the central sulcus according to the literature (Hari and Forss 1999) or reasonably close. We defined the putative source from HD-EEG as a point in the brain-space with the maximum sLORETA intensity. We refer to this point simply (while being aware of this oversimplification) as a “HD-EEG source” and to the distance from this point as a “HD-EEG source-distance”. Thus, the HD-EEG sLORETA source localization was taken as the reference point (“the ground truth”) to which both the sLORETA and ECD solutions from the SEEG were compared.

For the sLORETA, the localization error was computed as the euclidean distance between the HD-EEG source and the maximum of source intensities obtained from SEEG (similar to (Dümpelmann et al. 2012)). For the ECD, the localization error was computed as the distance between the position of the best fitting dipole from SEEG and the HD-EEG source location.

The spatial overlap between HD-EEG and SEEG solutions was calculated using Dice coefficient defined as $2 \times X \cap Y / (X + Y)$ (Zou et al. 2004), where X and Y are the volumes of exported sLORETA solutions (voxel maps) for SEEG and HD-EEG. The sLORETA voxel maps were thresholded above 95% of so-called *robust range function* used in FMRIB’s Software Library (FSL), and essentially computed from the range between 2nd and 98th percentiles

of voxel intensities (Smith et al. 2004). We set this spatial threshold to 95% robust range of the maximum sLORETA activation, because the spatial extent of sLORETA solutions tend to be overestimated and focal sources show up clearly only for high thresholds, e.g. above 90% (Cosandier-Rimele et al. 2017). We would like to note that comparison of spatial source extent from SEEG and HD-EEG can be biased due to the essentially different SNRs of the two signals, which may, in principle, result in two very different distributions of the spatial extent. Thus, we first statistically compared the spatial volumes between SEEG and HD-EEG.

Extracted Variables from the SEEG

From the recorded SEEG signal, we extracted eight different parameters, to investigate their correlation with the ESI results. (A) a number of “highly activated” ($> 10 \mu\text{V}$) SEEG contacts; (B) a number of different electrodes with “highly activated” contacts; (C) maximal value of SEEG SEP amplitude; (D) maximal value of SEEG SEP SNR; (E) spatial conditioning ratio of the SEEG contact positions around the HD-EEG source; (F) distance from the HD-EEG source to the nearest contact; (G) distance from the HD-EEG source to the “most activated” SEEG contact; (H) distance from the HD-EEG source to the contact with maximal SNR. All values were taken at the time of ESI computation. Here, we make a distinction between SEEG “contacts” and SEEG “electrodes” (one electrode consists of multiple collinear contacts; a channel is a recorded contact). We defined “highly activated” SEEG contacts as those having the averaged absolute amplitude above $10 \mu\text{V}$ (a value above which it was possible to reliably distinguish SEP from the baseline noise). The “most activated” SEEG contact was defined as the one with the maximal absolute value of signal amplitude at the time of ESI computation (see Sect. [Time of Source Localization: SEEG and HD-EEG](#)). Another parameter was SNR, defined for each SEEG channel as squared mean of the SEP at the time of ESI computation divided by variance in the prestimulus baseline period:

$$SNR = \frac{(\text{mean}_{\text{trials}}(S))^2}{\text{var}_{\text{samples}}(B)},$$

where *trials* correspond to the filtered epochs of SEP (see Sect. [Signal Preprocessing \(Same for Both HD-EEG and SEEG\)](#)), S is the SEEG activity extracted at the time of ESI computation and B is the prestimulus baseline activity from all trials and samples in the time interval of $[-0.25, -0.1]$ s with respect to the median nerve stimulation onset ($=0$ s). Spatial conditioning ratio quantifies the spatial repartition of the SEEG contact positions around the putative source and was computed as the ratio between the longest and the

shortest axis of the ellipsoid from the principal component analysis (PCA), based on the formula in (Le Cam et al. 2019). The PCA was computed on the MNI coordinates of the SEEG contacts, the coregistration to MNI space was performed in Brainstorm. The different statistical tests are indicated in the text of the Results section. To account for multiple testing, we computed the false discovery rate (FDR) correction (Benjamini and Hochberg 1995).

Results

In this study, we aimed to assess the source localization of somatosensory evoked potentials (SEP) from SEEG signals under realistic experimental conditions. The SEEG ESI results were compared to the “ground truth” estimated by sLORETA from independent HD-EEG measurements in the same subjects. We computed the ESI for two different source localization algorithms: (1) the sLORETA and (2) the ECD. The comparison between the SEEG and HD-EEG ESI results was evaluated by source-distance (for both sLORETA and ECD) and spatial overlap for the sLORETA distributed source models (see Materials and Methods for more details).

Comparison of SEEG and HD-EEG Source Localizations

First, we systematically compared the SEP source localization obtained from SEEG and HD-EEG for all 20 patients with at least one electrode located in the contralateral hemisphere with respect to the stimulated hand. Thus, we present a total of 24 cases of stimulated SEP from 20 different patients (for example, patient P1 had a bilateral implantation, so we investigated both left and right hand median nerve stimulations). The localization results of the “ipsilateral cases” can be found in supplementary figure S1.

We focused on early time components of SEP. The mean (\pm SEM) timepoint when ESI was performed (see Sect. Time of Source Localization: SEEG and HD-EEG) for SEEG was 36 ± 3 ms (median = 33 ms) and for HD-EEG 42 ± 4 ms (median = 36 ms), where zero corresponds to the median nerve stimulation. The median of the absolute differences between localization timepoints for SEEG and HD-EEG was 5 ms.

Note that in the rest of the analyses below, we defined one, patient-specific “ground truth” source location, to which the SEEG ESI results (sLORETA and ECD) were compared. This “ground truth” was defined as the maximum sLORETA intensity from HD-EEG (Fig. 1). The distance between the HD-EEG sources estimated by sLORETA and ECD was (mean \pm SEM) 1.7 ± 0.2 cm (median = 1.7 cm). Although we carefully visually inspected the “ground truth” location based on known neuroanatomy of SEP (Hari and

Forss 1999; Lascano et al. 2014), it should be kept in mind that the “ground truth” location of the source in our study is only estimated (see Sect. The Number of SEEG Contacts/Electrodes for a more detailed discussion). We also detail one patient, showing the “ground truth” source position from the HD-EEG and a clear phase reversal of SEP in SEEG (see supplementary figure S5).

Both ESI methods converged to similar solutions for the SEEG signal, as there was a very high correlation between the sLORETA (Fig. 3, blue circles) and the ECD (Fig. 3, purple diamonds) source-distances (correlation coefficient $R = 0.96$, $P < 0.001$, Pearson correlation). Furthermore, there was also a strong negative correlation between the sLORETA localization error and spatial overlap of the HD-EEG and SEEG sources (Fig. 3, green stars): $R = -0.66$ ($P < 0.001$, Pearson correlation). The source volume for SEEG (mean \pm SD) was (2.9 ± 1.8) %, for HD-EEG: (2.2 ± 0.4) % with no significant difference between both signal modalities ($P = 0.23$, Wilcoxon rank sum test). The anti-correlation between distance and overlap underlines the validity of our results, as the smaller the distance between both sources (SEEG and HD-EEG), the higher the overlap.

There was also considerable variability in localization distances amongst the patients (Fig. 3), ranging from 0.4 to 10 cm. The variability of the localization results can primarily be accounted for by the differences in the implantation schemes with respect to the putative “ground truth” source. Note that in this study, we made no *a-priori* selection of patients based on their implantations, the position of the electrodes was defined solely by the needs of the clinical evaluation.

Remarkably, in almost 50% of the cases (11 out of 24 investigated stimulation sites), the localization accuracy was below 2 cm for both the sLORETA and the ECD methods.

As an exemplary result (Fig. 4), we illustrate the sLORETA localization result of a 33 years old male (P10 in Fig. 2) with hypermotor seizures who underwent frontal, bilateral symmetrical implantation with 6 electrodes on each side. In Fig. 4, we show concordant results of sLORETA ESI from both SEEG and HD-EEG with a localization error of 7 mm and spatial overlap of 69% in the right hemisphere, responding to the median nerve stimulation on the left wrist. Interestingly, there was only one electrode with “highly activated” contacts (amplitude > 10 μ V on 7 contacts) positioned near the central sulcus, while the others were clustered more anteriorly. Furthermore, in the supplementary material, we provide details of three other sLORETA results of selected patients: P12, LH (Fig. S2), illustrating a case that had two electrodes with “highly activated” contacts (amplitude > 10 μ V on 16 contacts of 2 different electrodes) and localization error = 16 mm; P11, LH (Fig. S3), illustrating a case with no “highly activated” electrodes (amplitude < 10 μ V, but the SEP was visually distinguishable from the prestimulus

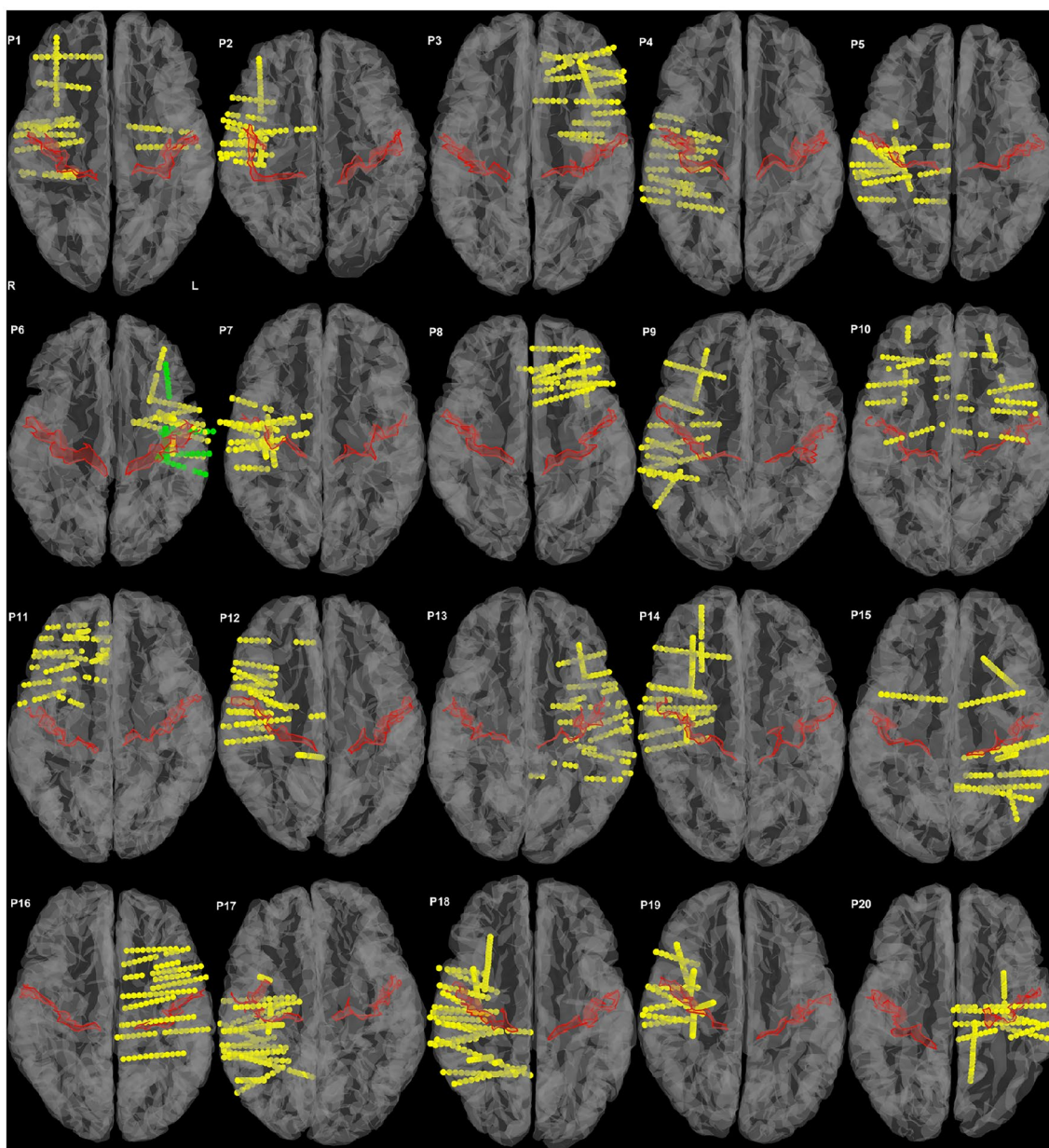


Fig. 2 Implantation schemes for all 20 patients based on individual MRI scans. Only those electrode contacts that were recorded and used in the ESI analysis are shown (yellow dots), explaining the gaps between contacts on some electrodes. The second implantation

in patient P6 (P6-2) is shown in green. The central sulcus, where the putative source of somatosensory evoked potentials is localized, was highlighted in red. The central sulcus was automatically located using the Destrieux atlas (Destrieux et al. 2010) implemented in CAT12

baseline activity) and localization error = 24 mm; P1, LH (Fig. S4), illustrating a case where the SEEG ESI failed (localization error = 56 mm, no visually detectable SEP).

Determinants of SEEG-Based ESI Localization

In the next step, we investigated which parameters of the SEEG recordings were related to the ESI results (Fig. 5). To this end, we selected 8 different parameters (columns

A-H of Fig. 5), which can hypothetically play a role in the SEEG source localization (see **Materials and Methods**, Sect. **Extracted Variables from the SEEG**):

We specifically selected 16 datasets with visually clearly distinguishable SEP in the SEEG signal (left from dashed red line in Fig. 3), having also a non-zero spatial overlap of the sLORETA solutions between SEEG and HD-EEG. The 10 μ V threshold of SEEG activation (selected based on visual aspection) identified the “highly

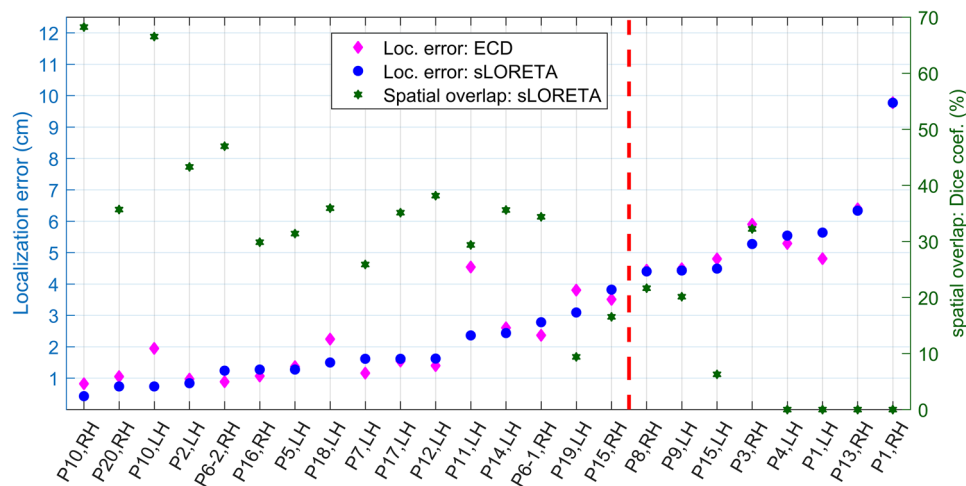


Fig. 3 SEEG-based ESI accuracy and spatial overlap for SEP source localization. The X-axis shows all patients (P1–P20) and the side of the median nerve stimulation (*LH* left hand, *RH* right hand). Only patients with contralateral hand stimulation and electrode implantations were included. The patients were sorted based on the localization distances from sLORETA. The ESI localization error (left Y-axis) was computed as the Euclidean distance between the HD-EEG source estimated by sLORETA (the “ground truth” source location) and the reconstructed sources from SEEG, based either on the sLORETA algorithm (blue dots) or the ECD method (purple dia-

monds). In the case of sLORETA, the source was defined as the voxel with the maximum of current density. The spatial overlap (green stars, right y-axis) between the sLORETA results from HD-EEG and SEEG was computed by the Dice coefficient from voxels, where the sLORETA intensity was larger than 95% of the robust range. Dashed red line then delineates 16 stimulation sites with visually clearly distinguishable SEP in SEEG. Notably, in 11 cases, the ESI localization accuracy was below 2 cm, demonstrating that in some cases ESI based on SEEG signal yields reliable source localization

activated” channels and the SEP value of 10 μV was also highly statistically significant in all cases (tested against the prestimulus baseline values of the SEEG SEP from the interval $[-0.25, -0.10]$ s, $P < 0.001$, Wilcoxon rank sum test, FDR corrected).

The parameter that correlated most and significantly (Pearson correlation, $P < 0.05$, FDR corrected) with the ESI localization errors was the distance from the HD-EEG source to the “most activated” SEEG contact (Fig. 5G). From the plot of the localization error of ECD (Fig. 5G, middle row), it could be speculated that the position of the dipole is the same as the position of the SEEG contact with maximal amplitude. Thus, we computed explicitly the distance between the dipole and the SEEG contact with max. amplitude: mean (\pm SD) distance was 0.8 ± 0.5 cm (range: 0.1–1.8 cm, median 0.7 cm).

Somewhat less correlated was the distance from HD-EEG source to the SEEG contact with the maximal SNR (Fig. 5H). Even less correlated was the distance from the HD-EEG source to the nearest SEEG contact. However, it should be noted that the HD-EEG source-distance to the “most activated” SEEG contact was highly correlated with the distance to the maximal SNR contact (correlation coefficient $R = 0.87$, $P < 0.001$), as well as with the distance to the nearest SEEG contact ($R = 0.81$, $P < 0.001$). In other words, the SEEG contacts that were most active, also

typically, had the maximal SNR and were often closest to the source. Rather surprisingly, the other parameters were not significantly correlated (see Discussion).

Changes in ESI After SEEG Electrode Rejection

To further investigate the role of the distance from the HD-EEG source to the most activated SEEG contact, we recomputed the ESI after omitting selected electrodes (Fig. 6). In the first round, we excluded one electrode with the most activated SEEG contact. In the second round, we rejected a second electrode with the next most activated SEEG contact. The ESI results for the different rejections were statistically evaluated by a sign test over the 16 SEP stimulation sites (left from the dashed line in Fig. 3) at the significance level $P = 0.05$ (FDR corrected).

Although after each rejection round, the ESI solution generally deteriorated (i.e., the overall localization error increased for both the sLORETA and the ECD, and the spatial overlap decreased), the differences were not significant (with the exception of the spatial overlap, which decreased significantly after rejection of two electrodes (Fig. 6A, lower plot)). This rather surprising lack of differences in localization errors after electrode rejection leverages the potential of SEEG-based ESI. Importantly, after each SEEG electrode rejection round, we found a strong and significant ($P < 0.05$,

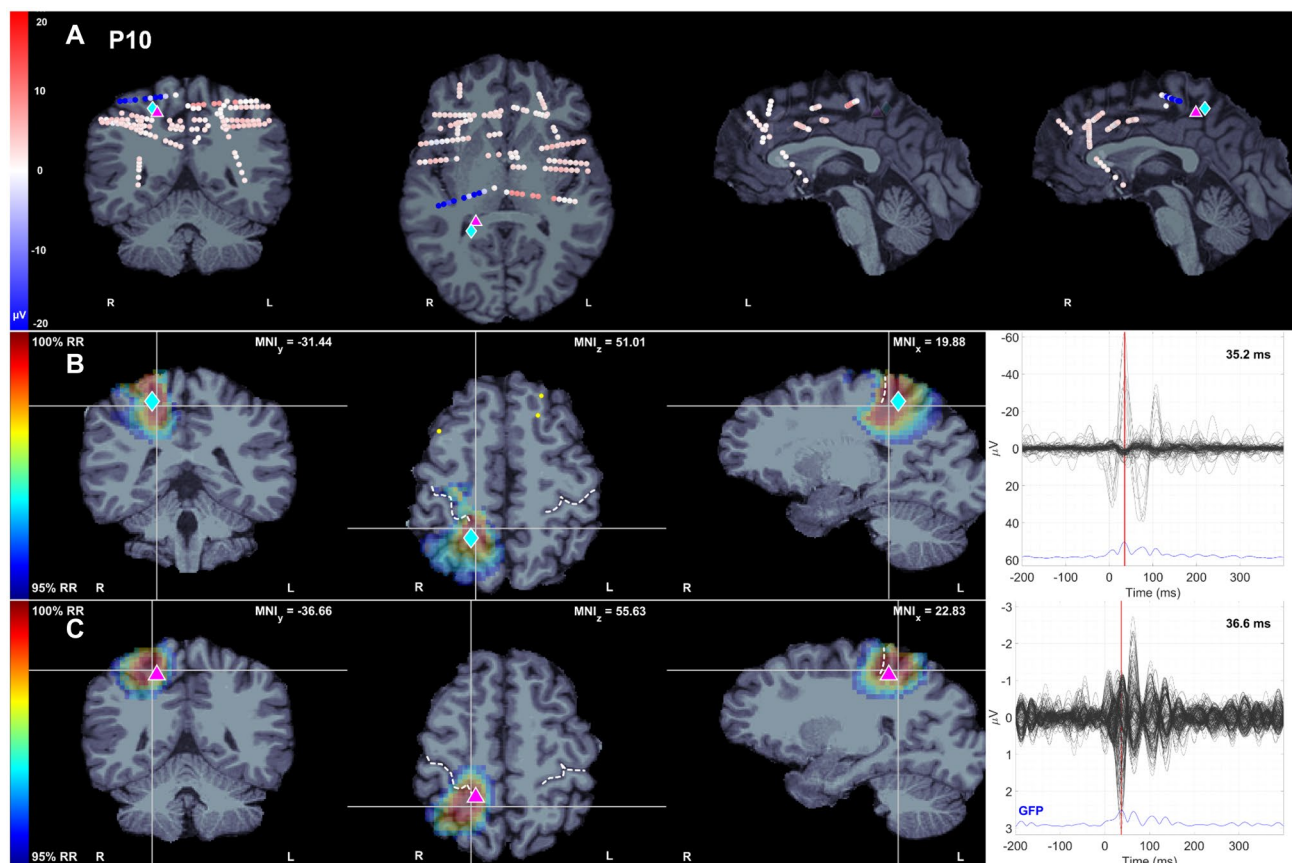


Fig. 4 Exemplary results of sLORETA source localization. A detailed overview of ESI based on SEP stimulation on the left hand of patient P10. **A** Axial, coronal and sagittal projections (from both sides of the mid-sagittal plane) of the used SEEG electrode contacts showing frontal, bilateral symmetric implantation (6 electrodes at the left and 6 at the right hemisphere). The amplitude scale cut-off at 20 μV . SEP sources in orthogonal slices estimated with sLORETA from **B** SEEG and **C** HD-EEG. The colour-coded values (left of B and C) were cut-off at 95% of the robust range of the sLORETA intensities (F-pseudo-statistic). Cross-hairs indicate the maximum values, MNI coordinates

shown in the picture. The position of the central sulcus is indicated by a dashed line. The blue diamond in B shows projections of the source maximum from the HD-EEG and the red triangle in C shows projections of the source maximum from the SEEG, for an easier comparison of the localization error. Corresponding averaged SEP of all channels (the so-called butterfly plots) filtered between 10–30 Hz are shown on the right of B and C with a red line indicating the time point used for source localization. The localization error was 7 mm and spatial overlap 69%

FDR corrected) correlation between the ESI results and the distance from the HD-EEG source to the most activated SEEG contact (Fig. 6B, C). Note that the distance from the HD-EEG source to the SEEG contact always changed in each rejection round of the electrode with the most activated contact. These results further underline the importance of the distance to the most activated contact for successful inverse solution based on SEEG signal.

Distance Between the Most Activated Contact and the SEEG Source

Another important question is how far from the electrodes is the source estimated from the SEEG? In the 11 best cases (Fig. 3), where the ESI yielded reliable results (i.e., localization error < 1.6 cm), the average distance

from the SEEG source to the nearest SEEG contact was 0.8 ± 0.2 cm (range 0.2–2.0 cm) for the sLORETA and 0.5 ± 0.1 cm (range 0.1–1.1 cm) for the ECD ESI. This indicates that under certain conditions—the SEEG-based source localization may yield reliable results beyond the immediate vicinity of the electrode contacts.

To gain a further insight into the relationship between the reconstructed SEEG source location and measured SEEG potential at the contacts, we investigated the potential distribution as a function of the distance from the reconstructed source (supplementary figure S6). Hypothetically, in case of very focal activations, we should see only a single peak at a certain distance from the source. However, the vast majority of the 16 cases show a multimodal, broad and rather complex distribution of the SEEG potential at multiple electrodes. We also detail three

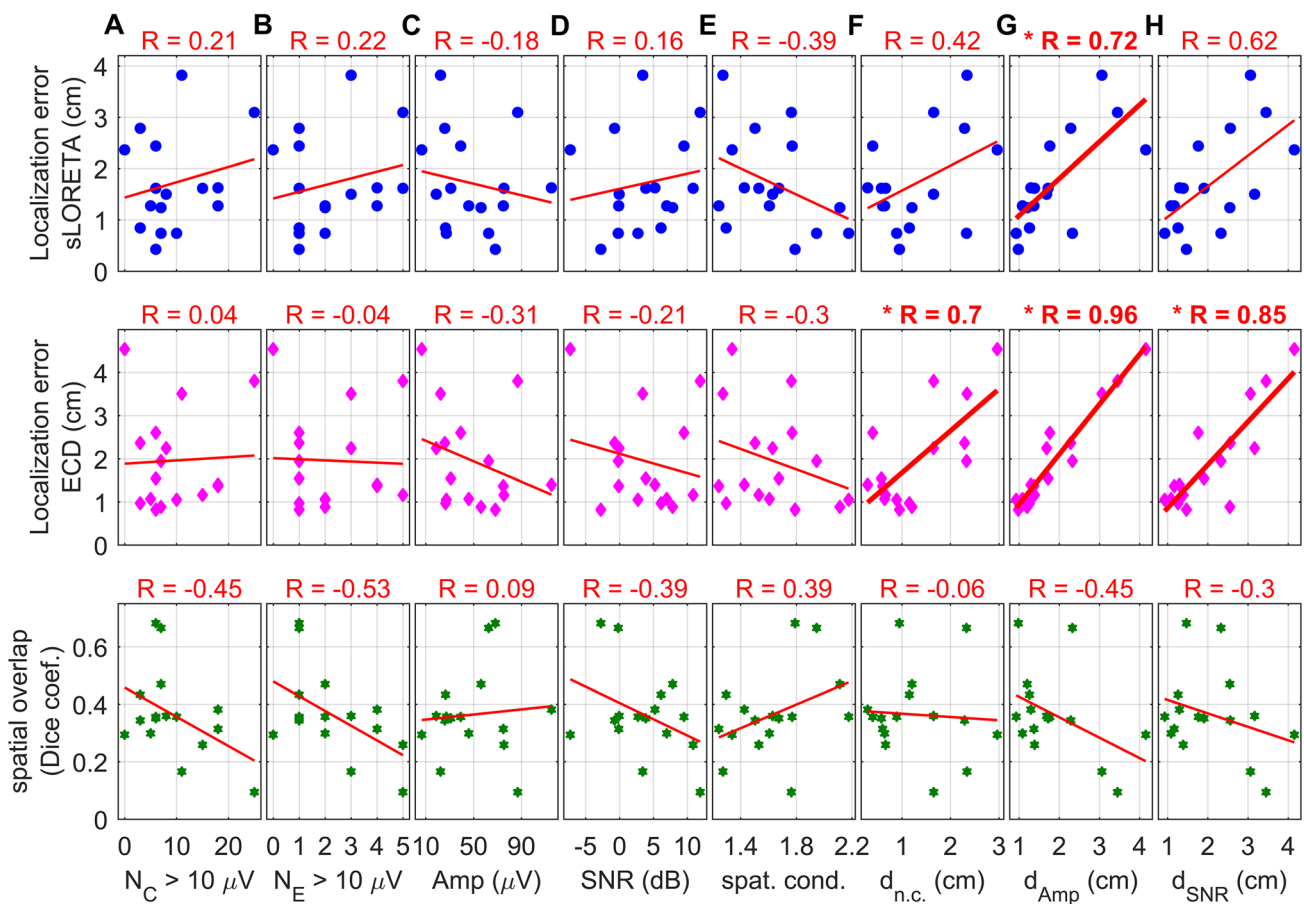


Fig. 5 Correlations of ESI accuracy and overlap with 8 different parameters of SEEG recordings. Rows represent the ESI results (Y-axes): first row—sLORETA localization error (blue dots), second row—ECD localization error (purple diamonds), third row—sLORETA spatial overlap between HD-EEG and SEEG sLORETA localizations (green stars) (third row). Columns represent the 8 different parameters of SEEG recordings (X-axes): **A** number of contacts and **B** number of different electrodes with activity above 10 μV at the time of ESI computation, **C** maximum amplitude (in absolute value) and **D** SNR of the SEEG signal at the time of ESI computa-

tion, **E** the spatial conditioning ratio of the SEEG contacts around the HD-EEG source, and distances from the HD-EEG source to **F** the nearest SEEG contact, **G** the most activated SEEG contact and **H** the SEEG contact with maximal SNR. Red stars indicate significant ($P < 0.05$, FDR corrected) Pearson correlation coefficients R (in red above each plot). Only the 16 cases with visually distinguishable SEPs (left from dashed red line in Fig. 3) were selected for statistical evaluations here. All values were taken at the time of ESI computation. The localization error correlated most with the distance from the HD-EEG source to the most activated SEEG contact

selected cases in supplementary figures S7–S9, showing how the SEEG source localization changed based on the electrode rejection.

During detailed checking of the localization results from the SEEG, we noticed an inverse relationship between the distance from the SEEG source to the most activated SEEG contact and the amplitude of the most activated SEEG contact: highly activated SEEG contacts had shorter distance to the reconstructed SEEG source than weakly activated ones. For example, if the SEEG SEP on the most activated contact was above 50 μV (a highly activated contact), then the source location reconstructed from the SEEG was only a few millimeters from that contact. On the contrary, if the SEEG SEP on the most activated contact was below 10 μV (a weakly activated contact), then the location of the SEEG

source was further away (a few centimeters). To verify this observation, we plotted the distances from the SEEG sources to the SEEG contacts with maximal amplitude (i.e., the absolute value of the SEP) as a function of the maximum SEEG amplitude value itself (Fig. 7). In this analysis, we also included the data from the SEEG electrode(s) rejection, because there the ESI was recomputed after excluding the contact with the previous maximal amplitude. We found a nonlinear relationship between the amplitude and the distance, which could be fit well by a low-order rational function in the form of $y = p/(x + q)$, with $R\text{-square} = 0.32$ and for the sLORETA (Fig. 7A) and 0.28 for the ECD (Fig. 7B). The P-values of the fits were statistically highly significant ($P < 0.001$).

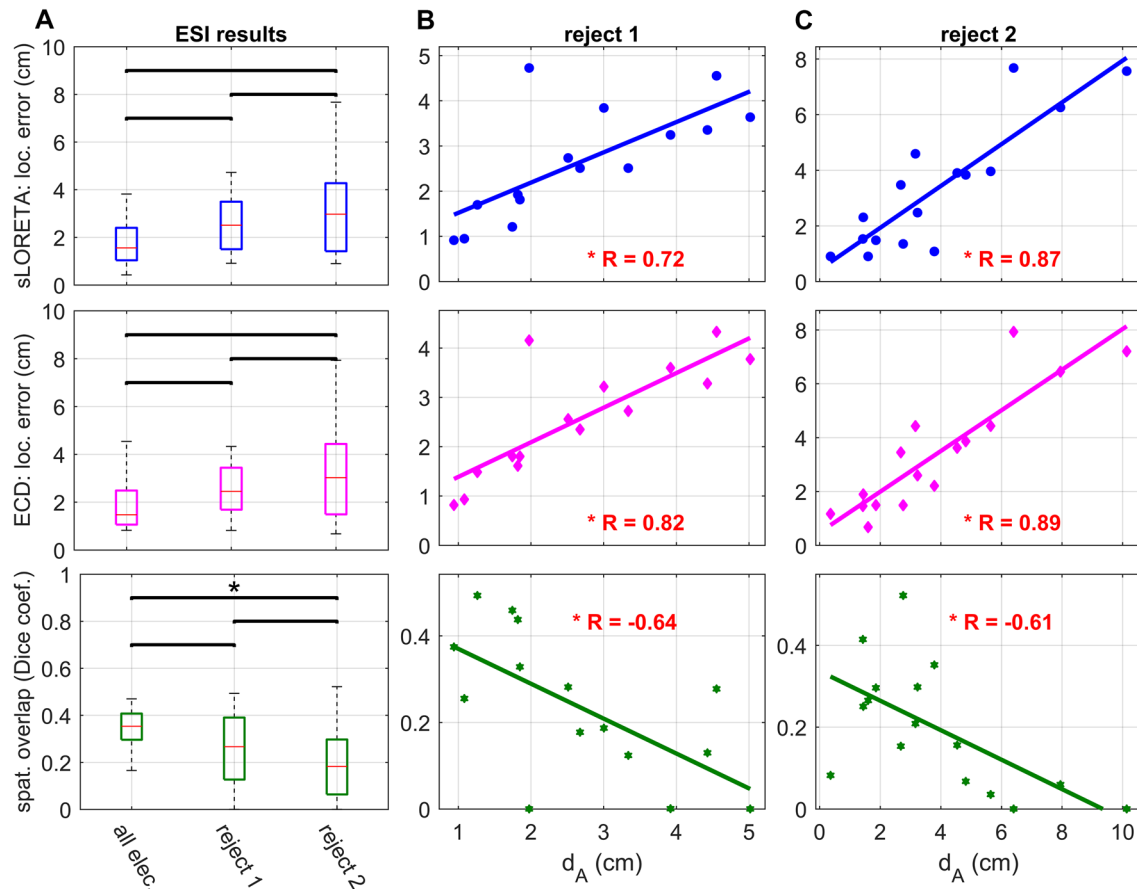


Fig. 6 ESI localizations after SEEG electrode rejection. We compared ESI for different SEEG electrode sets: the full set of SEEG contacts (all electrodes), rejection of one electrode with the most activated contact (reject 1), and rejection of two electrodes with the most activated contacts (reject 2). **A** ESI results: localization errors for sLORETA (top), ECD (middle) and spatial overlap (bottom). In each box-plot, the box indicates the interquartile range (IQR) of the localization error across the 16 stimulation sites, the median is marked by

a red, horizontal line inside the box, the whiskers indicate 1.5-times the IQR. Significant differences (sign test between the 16 values, $P < 0.05$, FDR corrected) are indicated by stars. Correlations between the ESI results (Y-axes) and the distance from HD-EEG source to the most activated SEEG contact (d_A) in the various SEEG electrode sets: **B** reject 1, **C** reject 2. One outlier value was rejected for 'reject 1'. Significant correlation coefficients R ($P < 0.05$, FDR corrected) are indicated by red stars and bold font

This means that for higher amplitude values, the distance of the reconstructed SEEG source was shorter from this SEEG contact, and vice versa. Notably, these results are only based on the SEEG measurements and ESI, independent of the source locations defined by the HD-EEG.

Discussion

In this study, we investigated the possibility of localizing neural sources from SEEG recordings of SEP as a physiological response. The source localization of SEEG from 20 epilepsy surgery patients using sLORETA and ECD

was compared to high-density EEG sLORETA results, representing the “ground truth” source location.

Summary of the Main Results

We show that under certain conditions, SEEG can reliably identify the onset source. Our main results can be summarized as follows: (i) SEEG sources (the results of the inverse solutions) can be localized beyond the SEEG contacts, (ii) SEEG ESI can lead to similar results to surface HD-EEG when the SEEG electrodes recorded sufficient information (e.g. distinguishable from the background activity), (iii) shorter distance (below 2 cm) of the most activated SEEG contacts from the putative “ground truth” source correlated

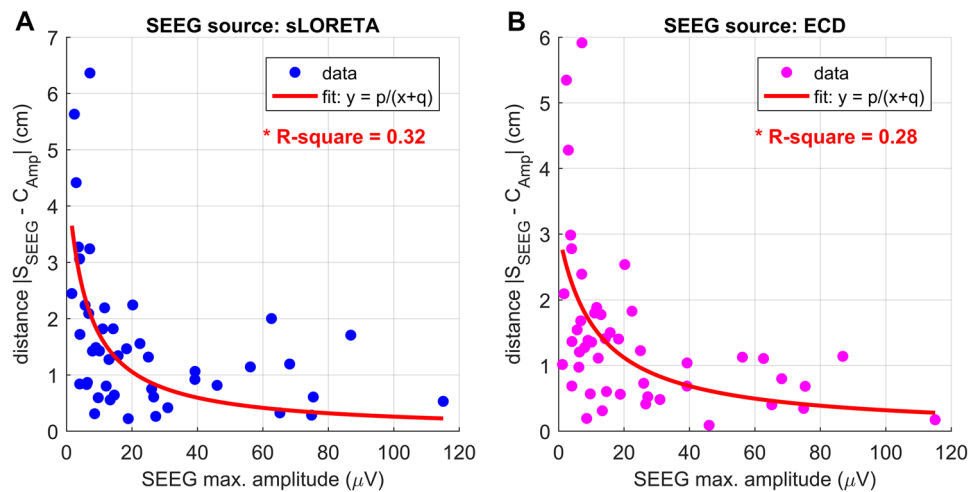


Fig. 7 Distance of SEEG sources to high-amplitude contacts. Dependency of distance from SEEG source (S_{SEEG}) to the contact with maximal amplitude (C_{Amp}) (Y-axis) on the value of that amplitude (X-axis). The SEEG amplitude was defined here as the absolute value of SEP. We selected a simple rational function to fit the data, $y = p/(x+q)$. Source reconstructions from **A** sLORETA

algorithm ($p=27$, $q=6$, N outliers=2) and **B** ECD algorithm ($p=36$, $q=12$, N outliers=1). In both cases, the fitted curves were able to explain a large portion of variance in the data ($P < 0.001$). The highly activated SEEG contacts influenced the inverse solutions from SEEG ESI more than weakly activated contacts

with lower localization error, and (iv) unduly activated SEEG contacts influenced the localization of the SEEG source towards that contact.

A weak point in most ESI studies based on iEEG recordings is their low sample size (i.e. the rather low number of reported patients). Several studies are restricted to single case reports (Caune et al. 2014; Dümpelmann et al. 2012; Le Cam et al. 2017; Zhang et al. 2008). Also others used a rather low sample size: $N=3$ (Yvert et al. 2005), $N=8$ (Lin et al. 2021), however, with notable exceptions: $N=14$ (Ramantani et al. 2013, 2014), $N=25$ (Alhilani et al. 2020). Here we reported source reconstructions from 42 stimulation sites (stimulation on both wrists of 20 patients, where one patient was implanted twice). For the detailed analysis (Figs. 5, 6 and 7), 16 stimulation sites from 14 different patients were taken into account.

Determinants of SEEG ESI Localization

We achieved localization errors below 16 mm, a value often reported as a reliable source reconstruction result (Dümpelmann et al. 2012), in about 50% (11/24 stimulation sites) for sLORETA, 38% (9/24) for ECD and a spatial overlap larger than 50% in more than half (14/24) of investigated cases (Fig. 3). Overall, we observed a wide range of localization errors, from 0.4 to 10 cm (Fig. 3), presumably because of the substantial spatial heterogeneity of the SEEG implantations, which were solely based on clinical indication and not for the purpose of this study. While such heterogeneity

is an inherent limitation to most SEEG studies hampering the inter-subject comparison (Lin et al. 2021), it can also be an advantage in correlation analysis for verifying which parameters of the SEEG recording are contributing to the ESI results; the primary aim of this study.

Proximity of the SEEG Contacts to the Reconstructed Source

Interestingly, nearly all the studies on iEEG-based ESI arrived at a similar conclusion that the iEEG-based ESI only yields good results, if the recording electrode contacts are “sufficiently” close to the source—typically only a few centimeters (Dümpelmann et al. 2009, 2012; Caune et al. 2013; Chang et al. 2005; Le Cam et al. 2014; Hosseini et al. 2018). In the ECoG, reliable reconstructions (< 1.5 cm) were possible only if the sources were close to the recording electrode contacts (Dümpelmann et al. 2012). Sources further from the electrodes and/or more distributed sources were rather poorly localized as to their spatial extent (Cosandier-Rimele et al. 2017). Todaro and colleagues showed that localization error increased linearly with distance from the electrodes (Todaro et al. 2019). Similarly in SEEG, Le Cam and co-workers reported reliable localizations (< 1 cm) if the close contacts were less than 2.5 cm away from the source (Le Cam et al. 2014). In a recent study, Lin and colleagues showed that the SNR of estimated neural currents strongly depended on the distance from the electrode contact location (Lin et al. 2021).

In line with these studies, we also observed a strong linear relationship between the SEEG ESI localization error and

(i) the distance from the HD-EEG source to the most activated SEEG contact (Fig. 5G) or (ii) the distance from the HD-EEG source to the SEEG contact with maximal SNR (Fig. 5H). The added value here is that this is-to the best of our knowledge-the first confirmation of such a relationship based on physiological responses in a larger cohort of patients and not on numerical simulations.

In addition, we show that unduly activated SEEG contacts (i.e., highly activated relative to other contacts) were closer to the reconstructed SEEG ESI sources more than weakly activated contacts (Fig. 7). Thus, an interesting scenario to explore in future studies, would be to have balanced activity on multiple SEEG electrodes.

The Number of SEEG Contacts/Electrodes

Previously, the number of contacts to be used for a successful ESI from SEEG was investigated by Caune et al., who suggested that the quality of localization may be influenced by two factors: (1) using as many electrodes as possible and (2) as close as possible (Caune et al. 2014). Although the presumption that the higher the number of contacts/electrodes the better the source reconstruction seems evident, here neither the number of “highly activated” contacts nor the number of different electrodes with “highly activated” contacts yielded a significant correlation with our ESI results (Fig. 5A, B). Here, the “highly activated” contacts were defined as those with a clearly distinguishable signal (i.e., $> 10 \mu\text{V}$) from the prestimulus baseline period (see [Materials and Methods](#), Sect. [Extracted Variables from the SEEG](#)). We speculate that the inverse relationship between the SEEG amplitude and the distance of the SEEG source from the electrodes (Fig. 7) could explain the lack of correlation between the number of “highly activated” contacts or electrodes and the ESI accuracy (Fig. 5A, B): if a few contacts of one electrode were substantially more activated, then the role of the other contacts would be marginal (“shielded” by the highly activated contacts).

The Value of Maximal SEEG SEP Amplitude/SNR

We also investigated correlations between the ESI results and maximal amplitude (i.e., the absolute value of the SEP potential) or the maximal SNR in SEEG electrode contacts. In particular, SNR is a parameter that is frequently manipulated in simulation studies (Liu et al. 2005), where the signal is typically a mixture of a dipole signal and noise. For example, Caune et al. selected two different noise amplitudes and found significantly worse source reconstructions for the lower SNR (Caune et al. 2014). In our study, neither the maximal SNR nor the maximal amplitude of the SEEG SEP in each dataset correlated significantly with the localization error (Fig. 5C, D). This lack of correlation suggests that the

values of SNR (or amplitude) themselves is not predictive of the ESI accuracy, but that the geometrical aspects (the distances of the SEEG electrode contacts to the source or the arrangement of the SEEG electrode contacts around the source) play a critical role.

The Spatial Conditioning Ratio

Another parameter implicated to play a role in SEEG-based source reconstructions is the spatial conditioning ratio (Le Cam et al. 2019). Spatial conditioning quantifies a spatial balance of the implanted SEEG electrode contacts. For example, spherically distributed contacts around the putative source yield a value of the spatial conditioning ratio equal to 1, and high values for near-to-planar spatial arrangement of electrodes. The intuition behind this analysis is that a well-conditioned spatial arrangement (e.g., when the source is surrounded by a cloud of sensors) should yield better ESI results than a poorly conditioned one. In our ESI results, we observed decreasing localization accuracy with increasing spatial conditioning ratio, albeit not significant (Fig. 5E). Interestingly, in the aforementioned study of Le Cam et al., the authors showed that in the presence of noise, the ESI results were actually better for the spatial conditioning ratio in the range of 2–3 than in the range of 1–2. In our study, the spatial conditioning ratio ranged between 1.3 and 2.2 (Fig. 5E). A future study could attempt to combine the purely geometrical aspect, reflected by the spatial conditioning ratio, with the observed activations at the SEEG electrode contacts (for example by taking into account only the significantly activated SEEG contacts).

Limitations of Our Study

The main limitations of our study are discussed below.

Nonsimultaneous HD-EEG and SEEG Recordings

The HD-EEG and SEEG data were not acquired simultaneously, due to technical reasons, as the HD-EEG cap could not be worn after implantation of the SEEG electrodes. However, localization of the neural generator of the SEP response is considered to be consistent and reproducible over time (Schaefer et al. 2002).

Uncertainty in Location of the “ground truth” Source of SEP

Another limitation of our study is the localization of the putative source estimated with sLORETA from the HD-EEG (the “ground truth” location) to which the results from the SEEG ESI were compared. Estimates of localization error of sLORETA are in the range of 10–20 mm (Bradley et al. 2016; Liu et al. 2005). Such an uncertainty must be taken

into account when interpreting our results. To address this issue, we added noise to the localization error (Y-axes) in Fig. 5, which effectively modified the HD-EEG source-distance. The noise was drawn from a normal distribution (width equal to 20 mm at 3 sigma). We repeated this random noise addition to localization errors 100 times. Despite the added noise, we were able to reproduce the significant correlations between the distance from the HD-EEG source to the SEEG source and distance from the HD-EEG source to the most activated SEEG contact (cf. Fig. 5G) both for ECD ($R=0.84 \pm 0.01$, mean \pm SEM over the 100 repetitions, FDR-corrected $P < 0.05$ in 100% of the repetitions) and also for sLORETA ($R=0.63 \pm 0.01$, FDR-corrected $P < 0.05$ in 50% of the repetitions).

There are also other methods for putative source estimation, such as localization based on visual detection of *a-priori* well-known source positions in post-central sulcus, fMRI, direct cortical stimulation (DCS) or intraoperative recording of the SEP. However, some of these methods suffer from similar uncertainty in the source localizations, e.g. visual localization (Branco et al. 2003; Towle et al. 2003) or fMRI-based localization (Hammeke et al. 1994; Lascano et al. 2014). The DCS or intraoperative recordings of SEP were not exploited in our study, because the DCS did not evoke sensory responses in all patients, or not all patients underwent intraoperative recordings of SEP.

Sparse Electrode Coverage Near the Putative Source

Another drawback of this study, especially when transferring our results to clinical localization of epileptogenic networks, is the sporadic placement of SEEG contacts relative to the putative source, contrasting with the targeted placement in most of epilepsy implantations (Lie et al. 2015). Thus, to better generalize, a larger number of dense SEEG implantations around the putative source would be required.

Average Reference in iEEG Signals

In an ideal scenario, the reference channel would have a constant, null potential, which is, however, physically impossible, as there is no such point on the body (Nunez and Srinivasan 2006). Here, the iEEG signals were recorded against a reference channel located in the white matter and then re-referenced to their common average (i.e., mean over all non-rejected iEEG channels), similar to, for example, (Alhilani et al. 2020; Caune et al. 2014; Satzer et al. 2022). In fact, the common average reference is an “inbuilt” feature in Brainstorm toolbox computed prior to source localization and we employed the common average reference also in other data analysis (e.g., Fig. 5), for the sake of consistency. The common average reference signal in iEEG is, generally, due to its inhomogeneous sampling not zero, which could

influence some of our results, for example in determining the iEEG contact with maximal amplitude. However, we believe that the impact was rather small, also due to averaging over a large number of electrodes relatively far from the SEP source and averaging over a large number of the SEP trials in each patient. In particular, we computed the mean amplitude A (i.e., the absolute value of the 10–30 Hz filtered signal at the time of the ESI computation prior to the average re-referencing) of the used SEEG channels and of their common average. The common average reference ($A_{CAR} = 1.3 \pm 0.2 \mu\text{V}$, mean \pm SEM over the 24 cases with contralateral stimulation) was substantially smaller than the average amplitude of the SEEG contacts ($A_{SEEG} = 3.0 \pm 0.5 \mu\text{V}$, with a significant difference in distribution over the subjects: $P=0.01$, Wilcoxon rank sum test), and on the order of magnitude smaller than the amplitude of the most activated iEEG contact ($A_{MAX} = 18.9 \pm 5.6 \mu\text{V}$). The choice of reference electrode contact, reference montage and offline referencing has been subject to a long term debate (Hu et al. 2018; Mercier et al. 2022; Nunez et al. 1997; Yao et al. 2019). In iEEG clinical practice, the use of bipolar reference montage is very popular, but comes at the expense of potential subtraction of a distant source having the same impact on the electrode contact pair. Thus, other approaches were suggested to eliminate the influence of the reference electrode to facilitate results interpretation (Hu et al. 2008; Li et al. 2018; Madhu et al. 2012; McCarty et al. 2022).

SEP as Testbed for SEEG ESI

The SEP itself is a largely simplified setup, not well representative of complicated scenarios in real-world recordings with multiple active sources in the brain. We purposefully selected the early responses of the SEP after median nerve stimulation, because the early SEP responses have a well defined source location in the primary somatosensory cortex in postcentral gyrus (Hari and Forss 1999; Lascano et al. 2014). The well defined and *a-priori* known source location allowed us to check the validity of our results, especially in localizing the putative source estimated from the HD-EEG. On the other hand, the direct applicability of our results is limited to cases where a strong single source is present.

Choice of Frequency band

We used the frequency band between 10 and 30 Hz for SEP preprocessing (both for SEEG and HD-EEG). However, the frequency spectrum of SEP is much richer (Cheron et al. 2007), especially in the SEEG. In fact, there is no consensus on the proper choice of frequency band of SEP for ESI analysis in the literature. For example, other studies used different filter settings: 0.1–60 Hz (Christmann et al. 2002), 1–500 Hz (Towle et al. 2003), or 20–500 Hz (Grimm et al.

1998). Here we selected the 30 Hz upper bound of our band-pass filter for three reasons: first, we wanted to make sure that the 50 Hz line noise does not affect our results; second, the amplitudes of such high-frequency oscillations decrease due to the $1/f$ power law typical for EEG (Miller et al. 2009); third, we argue that the activity in frequencies above 30 Hz would cancel-out (or largely attenuate) in the averaged SEP, because the phases of such high-frequency oscillations would not be aligned with respect to the stimulus. The 10 Hz lower bound was set similar to other studies (Houzé et al. 2011; Lascano et al. 2014).

Choice of Localization Methods

In our study, we compared two different localization methods: (1) the underdetermined, spatially distributed sLORETA and (2) the overdetermined ECD. Both algorithms converged to similar solutions: the source localization errors for the sLORETA and ECD were highly correlated (Pearson correlation coefficient $R = 0.96$). Whether sLORETA or ECD are optimal for SEEG ESI, is an open question. The spatial coverage of SEEG differs considerably from scalp EEG or MEG, where ESI is commonly used. While scalp EEG electrodes (or MEG sensors) are relatively evenly distributed on the head surface, SEEG electrodes are colinear and uniquely distributed deep inside the brain around specific regions of interest. In scalp EEG, the sLORETA is widely used for its depth-weighting attribute and the spatial extent of the sLORETA inverse solution depends on these regularization parameters. While here we simply used the default settings in Brainstorm (Tadel et al. 2011), a future study could address their influence on the spatial overlap of the sources.

Future Directions

In future studies, it would be interesting to, not only, investigate the spatial locations of the sources, but also, to reconstruct the time-courses of the activations at these locations (Lin et al. 2021). Further possibilities to improve SEEG-based localization could be to restrict the source space to gray matter only (Le Cam et al. 2019) or exploit the finite element method (FEM) in construction of the forward model (Caune et al. 2014). Additionally, investigating more than a single generator of the neural activity would be valuable. Further pivotal research in SEEG-based ESI, would be to investigate in more detail the spatial arrangement of SEEG electrodes, especially in cases where multiple activated electrodes are surrounding the source. In SEEG studies with epilepsy patients, for ethical reasons, the positions of the electrodes must be guided by the needs of the clinical

evaluation. Hence, animal models will be invaluable for exploring the effects of different spatial arrangements of electrodes (Todaro et al. 2019).

Conclusions

SEEG-based ESI has far-reaching potential to change the way neural sources are localized, and may result in a shift from the current electrode contact-based analysis to computational source localizations. Several recent studies have brought encouraging results in this direction (Alhilani et al. 2020; Satzer et al. 2022) and here we add evidence that a successful localization of physiological neural sources (such as the SEP) from SEEG is feasible. On the other hand, the clinical applicability seems currently to be further limited to cases in which there is an appropriately proximate clinically-determined implant scheme. By investigating the conditions which determined the success of the localization, we confirmed that it is still desirable to have the contacts as close to the source as possible.

Supplementary Information The online version contains supplementary material available at <https://doi.org/10.1007/s10548-023-00994-5>.

Acknowledgements We would like to thank Dr. David Krysl for his thoughtful comments and all patients who participated in our study. Supported by GAUK 488217/2017 and GACR 20-21339 S.

Author Contributions AK: conceptualization, methodology, investigation, formal analysis, writing—original draft, visualization, funding acquisition. PJ: formal analysis, data curation. PF: investigation, writing—review & editing. PM: conceptualization, resources, writing—review & editing, supervision, funding acquisition. JH: conceptualization, methodology, investigation, writing—original draft, formal analysis.

Data Availability Due to patient privacy restrictions, raw data is available from the corresponding author on reasonable request ensuring data privacy. For ESI, we used the Brainstorm package, version May 2021 (see [Materials and Methods](#) for more details). The software code for further analysis and image reconstruction are available from the corresponding author on request.

Declarations

Conflict of interest The authors declare that they have no conflict of interest.

Ethical Approval The study was reviewed and approved by the Ethics Committee of Motol University Hospital (No. 488217, 31/10/2016). Written informed consent to participate in this study was obtained from all the subjects.

References

- Alhilani M, Tamilia E, Ricci L, Ricci L, Grant PE, Madsen JR, Pearl PL, Papadelis C (2020) Ictal and interictal source imaging on intracranial EEG predicts epilepsy surgery outcome in children with focal cortical dysplasia. *Clin Neurophysiol* 131(3):734–743. <https://doi.org/10.1016/j.clinph.2019.12.408>
- Bai X, Towle VL, He EJ, He B (2007) Evaluation of cortical current density imaging methods using intracranial electrocorticograms and functional MRI. *NeuroImage* 35(2):598–608. <https://doi.org/10.1016/j.neuroimage.2006.12.026>
- Bastin J, Deman P, David O, Gueguen M, Benis D, Minotti L, Hoffman D, Combrisson E, Kujala J, Perrone-Bertolotti M, Kahane P, Lachaux J-P, Jerbi K (2017) Direct recordings from human anterior insula reveal its leading role within the error-monitoring network. *Cereb Cortex* 27(2):1545–1557. <https://doi.org/10.1093/cercor/bhv352>
- Benjamini Y, Hochberg Y (1995) Controlling the false Discovery rate: a practical and powerful approach to multiple testing. *J Roy Stat Soc: Ser B (Methodol)* 57(1):289–300. <https://doi.org/10.1111/j.2517-6161.1995.tb02031.x>
- Bradley A, Yao J, Dewald J, Richter C-P (2016) Evaluation of electroencephalography source localization algorithms with multiple cortical sources. *PLoS ONE* 11(1):e0147266. <https://doi.org/10.1371/journal.pone.0147266>
- Branco DM, Coelho TM, Branco BM, Schmidt L, Calcagnotto ME, Portuguese M, Neto EP, Paglioli E, Palmi A, Lima JV, Da Costa JC (2003) Functional variability of the human cortical motor map: electrical stimulation findings in perirolandic epilepsy surgery. *J Clin Neurophysiol: Off Publ Am Electroencephalogr Soc* 20(1):17–25. <https://doi.org/10.1097/00004691-200302000-00002>
- Caune V, Le Cam S, Ranta R, Maillard L, Louis-Dorr V (2013) Dipolar source localization from intracerebral SEEG recordings. 35th annual international conference of the IEEE engineering in medicine and biology society (EMBC). <https://doi.org/10.1109/EMBC.2013.6609432>
- Caune V, Ranta R, Le Cam S, Hofmanis J, Maillard L, Koessler L, Louis-Dorr V (2014) Evaluating dipolar source localization feasibility from intracerebral SEEG recordings. *NeuroImage* 98:118–133. <https://doi.org/10.1016/j.neuroimage.2014.04.058>
- Chang N, Gulrajani R, Gotman J (2005) Dipole localization using simulated intracerebral EEG. *Clin Neurophysiol* 116(11):2707–2716. <https://doi.org/10.1016/j.clinph.2005.07.002>
- Cheron G, Cebolla AM, De Saedeleer C, Bengoetxea A, Leurs F, Leroy A, Dan B (2007) Pure phase-locking of beta/gamma oscillation contributes to the N30 frontal component of somatosensory evoked potentials. *BMC Neurosci* 8(1):75. <https://doi.org/10.1186/1471-2202-8-75>
- Cho J-H, Hong SB, Jung Y-J, Kang H-C, Kim HD, Suh M, Jung K-Y, Im C-H (2011) Evaluation of algorithms for intracranial EEG (iEEG) source imaging of extended sources: feasibility of using iEEG source imaging for localizing epileptogenic zones in secondary generalized epilepsy. *Brain Topogr* 24(2):91–104. <https://doi.org/10.1007/s10548-011-0173-2>
- Christmann C, Ruf M, Braus DF, Flor H (2002) Simultaneous electroencephalography and functional magnetic resonance imaging of primary and secondary somatosensory cortex in humans after electrical stimulation. *Neurosci Lett* 333(1):69–73. [https://doi.org/10.1016/S0304-3940\(02\)00969-2](https://doi.org/10.1016/S0304-3940(02)00969-2)
- Cosandier-Rimele D, Ramantani G, Zentner J, Schulze-Bonhage A, Dümpelmann M (2017) A realistic multimodal modeling approach for the evaluation of distributed source analysis: application to sLORETA. *J Neural Eng* 14(5):056008. <https://doi.org/10.1088/1741-2552/aa7db1>
- Dahnke R, Yotter RA, Gaser C (2013) Cortical thickness and central surface estimation. *NeuroImage* 65:336–348. <https://doi.org/10.1016/j.neuroimage.2012.09.050>
- Destrieux C, Fischl B, Dale A, Halgren E (2010) Automatic parcellation of human cortical gyri and sulci using standard anatomical nomenclature. *NeuroImage* 53(1):1–15. <https://doi.org/10.1016/j.neuroimage.2010.06.010>
- Dümpelmann M, Fell J, Wellmer J, Urbach H, Elger CE (2009) 3D source localization derived from subdural strip and grid electrodes: a simulation study. *Clin Neurophysiol* 120(6):1061–1069. <https://doi.org/10.1016/j.clinph.2009.03.014>
- Dümpelmann M, Ball T, Schulze-Bonhage A (2012) SLORETA allows reliable distributed source reconstruction based on subdural strip and grid recordings. *Hum Brain Mapp* 33(5):1172–1188. <https://doi.org/10.1002/hbm.21276>
- George DD, Ojemann SG, Drees C, Thompson JA (2020) Stimulation mapping using stereoelectroencephalography: current and future directions. *Front Neurol* 11:320. <https://doi.org/10.3389/fneur.2020.00320>
- Gramfort A, Papadopoulos T, Olivi E, Clerc M (2010) OpenMEEG: opensource software for quasistatic bioelectromagnetics. *Biomed Eng Online* 9(1):45. <https://doi.org/10.1186/1475-925X-9-45>
- Grimm C, Schreiber A, Kristeva-Feige R, Mergner T, Hennig J, Lücking CH (1998) A comparison between electric source localisation and fMRI during somatosensory stimulation. *Electroencephalogr Clin Neurophysiol* 106(1):22–29. [https://doi.org/10.1016/S0013-4694\(97\)00122-3](https://doi.org/10.1016/S0013-4694(97)00122-3)
- Hämäläinen M, Hari R, Ilmoniemi RJ, Knuutila J, Lounasmaa OV (1993) Magnetoencephalography—theory, instrumentation, and applications to noninvasive studies of the working human brain. *Rev Mod Phys* 65(2):413–497. <https://doi.org/10.1103/RevModPhys.65.413>
- Hammeke TA, Yetkin FZ, Mueller WM, Morris GL, Haughton VM, Rao SM, Binder JR (1994) Functional magnetic resonance imaging of somatosensory stimulation. *Neurosurgery* 35(4):677–681. <https://doi.org/10.1227/00006123-199410000-00014>
- Hari R, Forss N (1999) Magnetoencephalography in the study of human somatosensory cortical processing. *Philos Trans Royal Soc Lond Ser B: Biol Sci* 354(1387):1145–1154. <https://doi.org/10.1098/rstb.1999.0470>
- Hosseini SAH, Sohrabpour A, He B (2018) Electromagnetic source imaging using simultaneous scalp EEG and intracranial EEG: an emerging tool for interacting with pathological brain networks. *Clin Neurophysiol* 129(1):168–187. <https://doi.org/10.1016/j.clinph.2017.10.027>
- Houzé B, Perchet C, Magnin M, Garcia-Larrea L (2011) Cortical representation of the human hand assessed by two levels of high-resolution EEG recordings. *Hum Brain Mapp* 32(11):1894–1904. <https://doi.org/10.1002/hbm.21155>
- Hu S, Stead M, Worrell GA (2008) Removal of scalp reference signal and line noise for intracranial EEGs. IEEE international conference on networking, sensing and control, 1486–1491. <https://doi.org/10.1109/ICNSC.2008.4525455>
- Hu S, Lai Y, Valdes-Sosa PA, Bringas-Vega ML, Yao D (2018) How do reference montage and electrodes setup affect the measured scalp EEG potentials? *J Neural Eng* 15(2):026013. <https://doi.org/10.1088/1741-2552/aaa13f>
- Isnard J, Taussig D, Bartolomei F, Bourdillon P, Catenoux H, Chassoux F, Chipaux M, Clémenceau S, Colnat-Coulbois S, Denuelle M, Derrey S, Devaux B, Dorfmueller G, Gilard V, Guenot M, Job-Chapron A-S, Landré E, Lebas A, Maillard L, Sauleau P (2018) French guidelines on stereoelectroencephalography (SEEG). *Neurophysiol Clin* 48(1):5–13. <https://doi.org/10.1016/j.neucli.2017.11.005>
- Koessler L, Benar C, Maillard L, Badier J-M, Vignal JP, Bartolomei F, Chauvel P, Gavaret M (2010) Source localization of ictal epileptic

- activity investigated by high resolution EEG and validated by SEEG. *NeuroImage* 51(2):642–653. <https://doi.org/10.1016/j.neuroimage.2010.02.067>
- Korzyukov O, Pflieger ME, Wagner M, Bowyer SM, Rosburg T, Sundaresan K, Elger CE, Boutros NN (2007) Generators of the intracranial P50 response in auditory sensory gating. *NeuroImage* 35(2):814–826. <https://doi.org/10.1016/j.neuroimage.2006.12.011>
- Lascano AM, Grouiller F, Genetti M, Spinelli L, Seeck M, Schaller K, Michel CM (2014) Surgically relevant localization of the central sulcus with high-density somatosensory-evoked potentials compared with functional magnetic resonance imaging. *Neurosurgery* 74(5):517–526. <https://doi.org/10.1227/NEU.0000000000000298>
- Le Cam S, Caune V, Ranta R, Maillard L, Koessler L, Louis-Dorr V (2014) Influence of the stereo-EEG sensors setup and of the averaging on the dipole localization problem. 36th annual international conference of the IEEE Engineering in medicine and biology society 1147–1150. <https://doi.org/10.1109/EMBC.2014.6943798>
- Le Cam S, Ranta R, Caune V, Korats G, Koessler L, Maillard L, Louis-Dorr V (2017) SEEG dipole source localization based on an empirical bayesian approach taking into account forward model uncertainties. *NeuroImage* 153:1–15. <https://doi.org/10.1016/j.neuroimage.2017.03.030>
- Le Cam S, Caune V, Ranta R, Louis-Dorr V (2019) Dealing with the SEEG sparse setup: a local dipole fitting strategy. 9th international IEEE/EMBS conference on neural engineering (NER) 1003–1006. <https://doi.org/10.1109/NER.2019.8716898>
- Lee E-K, Seyal M (1998) Generators of short latency human somatosensory-evoked potentials recorded over the spine and scalp. *J Clin Neurophysiol* 15(3):227–234
- Li G, Jiang S, Paraskevopoulou SE, Wang M, Xu Y, Wu Z, Chen L, Zhang D, Schalk G (2018) Optimal referencing for stereo-electroencephalographic (SEEG) recordings. *NeuroImage* 183:327–335. <https://doi.org/10.1016/j.neuroimage.2018.08.020>
- Lie OV, Papanastassiou AM, Cavazos JE, Szabo CA (2015) Influence of intracranial electrode density and spatial configuration on interictal spike localization: a case study. *J Clin Neurophysiol* 32(5):E30–E40. <https://doi.org/10.1097/WNP.0000000000000153>
- Lin F-H, Lee H-J, Ahveninen J, Jääskeläinen IP, Yu H-Y, Lee C-C, Chou C-C, Kuo W-J (2021) Distributed source modeling of intracranial stereo-electro-encephalographic measurements. *NeuroImage* 230:117746. <https://doi.org/10.1016/j.neuroimage.2021.117746>
- Liu H, Schimpf PH, Dong G, Gao X, Yang F, Gao S (2005) Standardized shrinking LORETA-FOCUSS (SSLOFO): a new algorithm for spatio-temporal EEG source reconstruction. *IEEE Trans Biomed Eng* 52(10):1681–1691. <https://doi.org/10.1109/TBME.2005.855720>
- Madhu N, Ranta R, Maillard L, Koessler L (2012) A unified treatment of the reference estimation problem in depth EEG recordings. *Med Biol Eng Comput* 50(10):1003–1015. <https://doi.org/10.1007/s11517-012-0946-0>
- Mai JK, Majtanik M, Paxinos G (2016) Atlas of the human brain, 4th edn. Elsevier, Amsterdam
- McCarty MJ, Woolnough O, Mosher JC, Seymour J, Tandon N (2022) The listening zone of human electrocorticographic field potential recordings. *ENeuro*. <https://doi.org/10.1523/ENEURO.0492-21.2022>
- Mercier MR, Dubarry A-S, Tadel F, Avanzini P, Axmacher N, Cellier D, Vecchio MD, Hamilton LS, Hermes D, Kahana MJ, Knight RT, Llorens A, Megevand P, Melloni L, Miller KJ, Piai V, Puce A, Ramsey NF, Schwiedrzik CM, Oostenveld R (2022) Advances in human intracranial electroencephalography research, guidelines and good practices. *NeuroImage* 260:119438. <https://doi.org/10.1016/j.neuroimage.2022.119438>
- Michel CM, Brunet D (2019) EEG source imaging: a practical review of the analysis steps. *Front Neurol*. <https://doi.org/10.3389/fneur.2019.00325>
- Michel CM, Murray MM, Lantz G, Gonzalez S, Spinelli L, de Grave R (2004) EEG source imaging. *Clin Neurophysiol* 115(10):2195–2222. <https://doi.org/10.1016/j.clinph.2004.06.001>
- Miller KJ, Sorensen LB, Ojemann JG, Den Nijs M (2009) Power-law scaling in the brain surface electric potential. *PLOS Comput Biol* 5(12):e1000609. <https://doi.org/10.1371/journal.pcbi.1000609>
- Minotti L, Montavont A, Scholty J, Tyvaert L, Taussig D (2018) Indications and limits of stereoelectroencephalography (SEEG). *Neurophysiol Clinique = Clinical Neurophysiol* 48(1):15–24. <https://doi.org/10.1016/j.neucli.2017.11.006>
- Nunez PL, Srinivasan R (2006) Electric Fields of the brain: the Neurophysics of EEG. Oxford University Press, Oxford
- Nunez PL, Srinivasan R, Westdorp AF, Wijesinghe RS, Tucker DM, Silberstein RB, Cadusch PJ (1997) EEG coherency: I: statistics, reference electrode, volume conduction, laplacians, cortical imaging, and interpretation at multiple scales. *Electroencephalogr Clin Neurophysiol* 103(5):499–515. [https://doi.org/10.1016/S0013-4694\(97\)00066-7](https://doi.org/10.1016/S0013-4694(97)00066-7)
- Papademetris X, Jackowski MP, Rajeevan N, DiStasio M, Okuda H, Constable RT, Staib LH (2006) BioImage suite: an integrated medical image analysis suite: an update. *Insight J* 2006:209
- Parvizi J, Kastner S (2018) Promises and limitations of human intracranial electroencephalography. *Nat Neurosci* 21(4):474–483. <https://doi.org/10.1038/s41593-018-0108-2>
- Pascarella A, Todaro C, Clerc M, Serre T, Piana M (2016) Source modeling of electrocorticography (ECoG) data: stability analysis and spatial filtering. *J Neurosci Methods* 263:134–144. <https://doi.org/10.1016/j.jneumeth.2016.02.012>
- Pascual-Marqui RD (2002) Standardized low resolution brain electromagnetic. *Clin Pharmacol* 16:5–12
- Pellegrino G, Hedrich T, Chowdhury RA, Hall JA, Dubeau F, Lina J-M, Kobayashi E, Grova C (2018) Clinical yield of magnetoencephalography distributed source imaging in epilepsy: a comparison with equivalent current dipole method. *Hum Brain Mapp* 39(1):218–231. <https://doi.org/10.1002/hbm.23837>
- Ramantani G, Cosandier-Riméle D, Schulze-Bonhage A, Maillard L, Zentner J, Dümpelmann M (2013) Source reconstruction based on subdural EEG recordings adds to the presurgical evaluation in refractory frontal lobe epilepsy. *Clin Neurophysiol* 124(3):481–491. <https://doi.org/10.1016/j.clinph.2012.09.001>
- Ramantani G, Dümpelmann M, Koessler L, Brandt A, Cosandier-Riméle D, Zentner J, Schulze-Bonhage A, Maillard LG (2014) Simultaneous subdural and scalp EEG correlates of frontal lobe epileptic sources. *Epilepsia* 55(2):278–288. <https://doi.org/10.1111/epi.12512>
- Sammler D, Koelsch S, Ball T, Brandt A, Grigutsch M, Huppertz H-J, Knösche TR, Wellmer J, Widman G, Elger CE, Friederici AD, Schulze-Bonhage A (2013) Co-localizing linguistic and musical syntax with intracranial EEG. *NeuroImage* 64:134–146. <https://doi.org/10.1016/j.neuroimage.2012.09.035>
- Satzer D, Esengul YT, Warnke PC, Issa NP, Nordli DR (2022) SEEG in 3D: interictal source localization from intracerebral recordings. *Front Neurol* 13:782880. <https://doi.org/10.3389/fneur.2022.782880>
- Schaefer M, Mühlnickel W, Grüsser SM, Flor H (2002) Reproducibility and Stability of Neuroelectric Source Imaging in Primary Somatosensory Cortex. *Brain Topogr* 14:179–189. <https://doi.org/10.1023/A:1014598724094>
- Scherg M, Von Cramon D (1985) Two bilateral sources of the late AEP as identified by a spatio-temporal dipole model. *Electroencephalogr Clin Neurophysiol* 62(1):32–44. [https://doi.org/10.1016/0168-5597\(85\)90033-4](https://doi.org/10.1016/0168-5597(85)90033-4)

- Smith SM, Jenkinson M, Woolrich MW, Beckmann CF, Behrens TEJ, Johansen-Berg H, Bannister PR, De Luca M, Drobnjak I, Flitney DE, Niazy RK, Saunders J, Vickers J, Zhang Y, De Stefano N, Brady JM, Matthews PM (2004) Advances in functional and structural MR image analysis and implementation as FSL. *NeuroImage* 23:S208–S219. <https://doi.org/10.1016/j.neuroimage.2004.07.051>
- Tadel F, Baillet S, Mosher JC, Pantazis D, Leahy RM (2011) Brainstorm: a user-friendly application for MEG/EEG analysis. *Comput Int Neurosci*. <https://doi.org/10.1155/2011/879716>
- Tamilia E, AlHilani M, Tanaka N, Tsuboyama M, Peters JM, Grant PE, Madsen JR, Stufflebeam SM, Pearl PL, Papadelis C (2019) Assessing the localization accuracy and clinical utility of electric and magnetic source imaging in children with epilepsy. *Clin Neurophysiol* 130(4):491–504. <https://doi.org/10.1016/j.clinph.2019.01.009>
- Todaro C, Marzetti L, Sosa V, Valdes-Hernandez PA, P. A., Pizzella V (2019) Mapping brain activity with electrocorticography: resolution properties and robustness of inverse solutions. *Brain Topogr* 32(4):583–598. <https://doi.org/10.1007/s10548-018-0623-1>
- Towle VL, Khorasani L, Uftring S, Pelizzari C, Erickson RK, Spire J-P, Hoffmann K, Chu D, Scherg M (2003) Noninvasive identification of human central sulcus: a comparison of gyral morphology, functional MRI, dipole localization, and direct cortical mapping. *NeuroImage* 19(3):684–697. [https://doi.org/10.1016/S1053-8119\(03\)00147-2](https://doi.org/10.1016/S1053-8119(03)00147-2)
- Vlcek K, Fajnerova I, Nekovarova T, Hejtmanek L, Janca R, Jezdik P, Kalina A, Tomasek M, Krsek P, Hammer J, Marusic P (2020) Mapping the scene and object processing networks by intracranial EEG. *Front Hum Neurosci*. <https://doi.org/10.3389/fnhum.2020.561399>
- Völker M, Fiederer LDJ, Berberich S, Hammer J, Behncke J, Kršek P, Tomášek M, Marusič P, Reinacher PC, Coenen VA, Helias M, Schulze-Bonhage A, Burgard W, Ball T (2018) The dynamics of error processing in the human brain as reflected by high-gamma activity in noninvasive and intracranial EEG. *NeuroImage* 173:564–579. <https://doi.org/10.1016/j.neuroimage.2018.01.059>
- Yao D, Qin Y, Hu S, Dong L, Vega B, M. L., Valdés Sosa PA (2019) Which reference should we use for EEG and ERP practice? *Brain Topogr* 32(4):530–549. <https://doi.org/10.1007/s10548-019-00707-x>
- Yvert B, Fischer C, Bertrand O, Pernier J (2005) Localization of human supratemporal auditory areas from intracerebral auditory evoked potentials using distributed source models. *NeuroImage* 28(1):140–153. <https://doi.org/10.1016/j.neuroimage.2005.05.056>
- Zhang Y, van Drongelen W, Kohrman M, He B (2008) Three-dimensional brain current source reconstruction from intra-cranial ECoG recordings. *NeuroImage* 42(2):683–695. <https://doi.org/10.1016/j.neuroimage.2008.04.263>
- Zou KH, Warfield SK, Bharatha A, Tempany CMC, Kaus MR, Haker SJ, Wells WM, Jolesz FA, Kikinis R (2004) Statistical validation of image segmentation quality based on a spatial overlap index. *Acad Radiol* 11(2):178–189. [https://doi.org/10.1016/S1076-6332\(03\)00671-8](https://doi.org/10.1016/S1076-6332(03)00671-8)

Publisher's Note Springer nature remains neutral with regard to jurisdictional claims in published maps and institutional affiliations.

Springer Nature or its licensor (e.g. a society or other partner) holds exclusive rights to this article under a publishing agreement with the author(s) or other rightsholder(s); author self-archiving of the accepted manuscript version of this article is solely governed by the terms of such publishing agreement and applicable law.